Colloids and Surfaces B: Biointerfaces 160 (2017) 639–648

Contents lists available at ScienceDirect

Colloids and Surfaces B: Biointerfaces

journal homepage: www.elsevier.com/locate/colsurfb

Protocols

Direct one-pot synthesis of cinnamaldehyde immobilized on gold nanoparticles and their antibiofilm properties

Mohankandhasamy Ramasamy, Jin-Hyung Lee, Jintae Lee*

School of Chemical Engineering, Yeungnam University, Gyeongsan 38541, Republic of Korea

ARTICLE INFO

Article history:
Received 14 June 2017
Received in revised form
30 September 2017
Accepted 5 October 2017
Available online 6 October 2017

Keywords:
Cinnamaldehyde
Gold nanoparticles
Antibiofilm
C. albicans
Hyphal inhibition
Surface interactions

ABSTRACT

The objective of the present study was to develop a one-pot strategy to synthesis gold nanoparticle complexes using cinnamaldehyde, a potent antibiofilm agent which in its free form, exhibits high volatility and unstable nature. Hence, we developed cinnamaldehyde gold nanoparticles (CGNPs) in a single step to overcome the limitations of free cinnamaldehyde. Furthermore, reduction abilities of cinnamaldehyde under different experimental conditions, that is, varying precursor concentrations of cinnamaldehyde and gold, metal salts, pH, temperature, and light sources, were investigated. UV–vis spectroscopy, transmission electron microscopy, attenuated total reflectance Fourier transform infrared spectroscopy, and dynamic light-scattering measurements revealed that heat influenced the nanoparticle formation in the presence of cinnamaldehyde, and as produced cinnamaldehyde immobilized on gold nanoparticles were spherical, monodispersed, and stable by surface charge. CGNPs containing 0.01% cinnamaldehyde by weight exhibited effective biofilm inhibition of up to >80% against Gram positive bacteria (methicillin-sensitive and -resistant strains of *Staphylococcus aureus,* MSSA and MRSA, respectively) and Gram negative (*Escherichia coli* and *Pseudomonas aeruginosa*) and a fungus *Candida albicans*. In addition, CGNPs attenuated the virulence of *C. albicans* by inhibiting hyphae formation. Based on observations of their antibiofilm effects and confocal microscopy findings, CGNPs caused biofilm damage by direct contact. Thus, cinnamaldehyde appears to be a promising reduction material for the eco-friendly, one-pot synthesis of CGNPs with excellent antibiofilm activity.

1. Introduction

Infectious diseases induced by microbes constitute a huge challenge and continue to affect billions of people annually [1]. Furthermore, microbial resistance to and the ineffective wide-spectrum activities of conventional antibiotics result in high morbidity and mortality rates [2–4]. Biofilms are much more pathogenic than planktonic cells and are responsible for more than 80% of infectious diseases because of their presumed ability to confer resistance to pathogens by restricting exposure to antibiotics, which is accomplished by the production of extracellular polymeric substances (EPS), the induction of multi-drug efflux pumps, and the presence of persister cells [5–7]. Accordingly, it is important alternative antimicrobial agents capable of inhibiting microbial growth and biofilms be developed to control infections, and nanotechnology appears to be well poised to meet this challenge.

Nanoscale noble metals, especially gold, have fascinated researchers due to their unique optical, electronic, catalytic and magnetic properties, which are often fundamentally different from those of their bulk counterparts due to their diminutive sizes and surface effects [8–10]. However, the chemical and physical techniques current used to synthesize gold nanoparticle (GNPs) require the use of toxic, expensive chemicals as reducing agents, stabilizing agents, and as solvent systems, and these pose risks to both the environmental and health [11,12]. Biosynthetic methods using plant extracts have received more attention than physically, chemically, and even microbially based methods of synthesis, which all require an aseptic environment for the production of nano-scale metals. As a result, one-pot synthetic methods based on phytochemicals that overcome the difficulties of multi-pot processes, which include long reaction times, the use of harmful chemicals, particle agglomeration, crystal deformation, scale-up difficulties, toxicity issues, and production cost [13]. Therefore, facile, rapid, eco-friendly, one-pot synthetic methods for producing nano-sized metals using phytochemicals are required.

Cinnamaldehyde is a bioactive compound found in the bark extract of the cinnamon tree and is currently used by the food

* Corresponding author.
E-mail address: jtlee@ynu.ac.kr (J. Lee).

https://doi.org/10.1016/j.colsurfb.2017.10.018
0927-7765/

preservation industry as a safe antimicrobial with U.S. Food and Drug Administration approval [14]. Cinnamaldehyde can destroy fungi cells, inhibit mold growth, and mycotoxin production by microbes [15]. However, its high volatility, instability, sparing water solubility, poor dispersability, its irritant effect, and its inability to reach target sites severely limit its biological applications [16–18]. We considered that cinnamaldehyde-mediated synthesis of nanocomplexes containing metal nanoparticles and cinnamaldehyde might provide a means of addressing these limitations.

In the present study, we describe the direct, one-pot, eco-friendly synthesis of cinnamaldehyde coated gold nanoparticles (CGNPs) using cinnamaldehyde as a green-reducing agent. The synthetic process used involved the optimization of conditions, that is, precursor concentration, pH, metal salts, and light sources. The CGNPs studied with respect to particle size, surface charge, surface functionalization and antimicrobial efficiency against Gram positive bacteria (methicillin-sensitive and -resistant strains of *Staphylococcus aureus,* MSSA and MRSA, respectively) and Gram negative (*Escherichia coli* and *Pseudomonas aeruginosa*) and a fungus *Candida albicans*.

2. Materials and methods

2.1. Microbial strains and growth conditions

The microbial strains used were enterohemorrhagic *Escherichia coli* (*E. coli*) O157:H7 [ATCC 43895, EDL933], *Pseudomonas aeruginosa* (*P. aeruginosa* PAO1), methicillin-sensitive *Staphylococcus aureus* (MSSA 6538) [ATCC 6538], methicillin-resistant *Staphylococcus aureus* (MRSA) [ATCC BAA-1707], and *Candida albicans* (*C. albicans* DAY 185). All the microbial experiments were conducted at 37 °C in Luria–Bertani (LB) medium for bacteria and in potato dextrose broth (PDB) for *C. albicans*. Initially, bacterial cells (stored at −80 °C in glycerol) were streaked on Luria-Bertani agar (LBA) plates at 37 °C. An overnight grown single colony was then inoculated into 25 ml of fresh LB broth in a 250 ml Erlenmeyer flask and incubated on a shaking incubator (at 250 rpm/min) for 24 h at 30 °C. In case of *C. albicans* (also stored at −80 °C in glycerol) was streaked on potato dextrose agar (PDA) plates and incubated at 37 °C for 48 h. A well grown single colony was then inoculated into 25 ml of PDB and cultured overnight at 37 °C. For phenotypic assays, stationary phase cells were re-inoculated into their respective media at an initial turbidity of 0.05 at 600 nm. All other chemicals utilized in this study were purchased from Sigma-Aldrich (St. Louis, USA).

The minimum inhibitory concentrations (MICs) of cinnamaldehyde, CGNPs, cinnamic acid, GNPs, SiGNPs and TGNPs were determined in 96-well polystyrene plates (SPL Life Sciences, Korea) using the standard broth microdilution method as prescribed by the Clinical and Laboratory Standards Institute (CLSI) protocol. Overnight grown bacteria or *C. albicans* cells were inoculated at a dilution of 1:100 in their respective media with serial twofold dilutions to yield final concentrations ranging from 0.005 to 0.5%, v v^{-1} or w v^{-1} of cinnamaldehyde or NPs, respectively. The MIC was determined to the lowest concentration that inhibited 80% microbial growth or no longer visible turbidity which was assessed by optical density readings at 600 nm using a Thermo Scientific Multiskan EX microplate reader (Thermo Fisher Scientific, Vantaa, Finland).

2.2. Green synthesis of cinnamaldehyde-gold nanoparticles (CGNPs)

A schematic of the method used is provided in Fig. 1a. Typically, CA was dissolved by vortexing in warm ethanol. Separately, $HAuCl_4{\cdot}4H_2O$ was added to 5 ml distilled water and kept on a hot water bath. CA and $HAuCl_4{\cdot}4H_2O$ solutions were mixed together with continuous stirring at 100 °C. The reaction mixture turned a ruby-red color within a minute, indicating CGNP formation, purified by dialysis, and stored at 4 °C for further use.

2.3. Influence of various parameters on CGNPs syntheses

The same experimental method was used to determine the effects of CA and $HAuCl_4{\cdot}4H_2O$ concentrations, pH, metal salts of $HAuCl_4{\cdot}4H_2O$ (Au), $AgNO_3$, (Ag), $CuSO_4$ (Cu), TiO_2 (Ti), and $Zn(NO_3)_2$ (Zn), and light (sunlight, UV light, visible light, and no light) on CGNP synthesis.

2.4. Characterizations of nanoparticles

The absorbance spectra of CGNPs were recorded between 200 and 700 nm using an UV–vis spectrophotometer (UV-1800, Shimadzu, Japan). A Zetasizer Nano ZS dynamic light-scattering (DLS) analyzer (Malvern Instruments, Malvern, UK) was used to determine particle sizes (nm) and zeta potentials (mV). Prior to UV–vis analysis, samples of synthesized nanoparticles were diluted 1000 times with ultrapure water. Results were the averages of 15 determinations.

Infrared spectra of CA and CGNPs were obtained using by attenuated total reflectance Fourier transform infrared spectroscopy (ATR-FTIR) using a Perkin-Elmer Spectrum Two® instrument at a resolution of 4 cm^{-1} (Perkin-Elmer Inc., Norwalk, CT, USA). Sixteen scans of spectra were collected and processed using Spectrum 10™ software.

Morphological features of CGNPs were investigated by high resolution transmission electron microscopy (HR-TEM, Tecnai G2 F20, FEI, USA) at an accelerating voltage of 200 kV. Before examinations, CGNPs dispersions were drop cast onto 300-mesh carbon coated TEM grids and air dried at room temperature.

Amount of cinnamaldehyde present in synthesized CGNPs were quantified using spectrophotometric method at 290 nm using UV–vis spectrophotometer (UV-1800, Shimadzu, Japan). Initially, using standard cinnamaldehyde stock solutions, a standard calibration curve was obtained which was linear in the range of 0.00025–0.1% v/v (data not shown) with a correlation coefficient of $R^2 = 0.999$. From this Beer and Lambert's law based calibration curve [19], the unknown concentration of cinnamaldehyde in CGNPs were calculated after intercepting the absorbance of CGNPs.

2.5. Quantification of biofilm inhibition by crystal violet assay

Static biofilm forming assays for bacteria and *C. albicans* were performed on 96-well polystyrene plates (SPL Life Sciences, Korea), as previously reported [20]. Briefly, microbes grown to the stationary phase were adjusted to an initial turbidity of 0.05 at 600 nm and co-cultured with or without bare gold nanoparticles (GNPs), ligand attached GNPs including silica coated GNPs (SiGNPs), tyrosine containing GNPs (TGNPs), and CGNPs at different concentrations (0–0.01%) in their respective media without shaking at 37 °C for 24 h. Cell growth at 620 nm was measured using a Thermo Scientific Multiskan EX (Thermo Fisher Scientific, Vantaa, Finland). Biofilm inhibition was quantified after copiously washing plates with distilled water to remove non-adherent cells, and staining with 300 μl of crystal violet (0.1%, v/v) for 20 min at room temperature. Plates were then washed three times with distilled water, blotted onto tissue paper towels, dried and extracted with ethanol (95%, v/v). Total biofilm formation was measured at 570 nm, and results are presented as the averages and standard deviations of at least three replicates. The significances of% biofilm formation

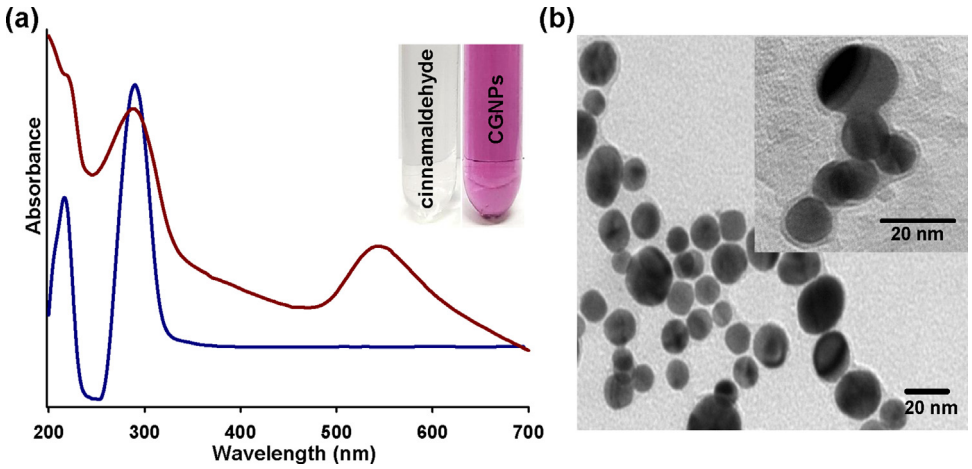

Fig. 1. UV–visible absorbance spectra (blue- cinnamaldehyde, red- CGNPs) of cinnamaldehyde reduced gold nanoparticles (CGNPs) produced at 100 °C (a), and TEM image showing the successful formation of CGNPs when cinnamaldehyde was used as a reducing agent (b); the inset image shows the cinnamaldehyde capping layer, which differs in contrast from the Au core (b).

differences were determined using the Student's *t*-test, and significance was accepted for p values of <0.05.

2.6. Confocal microscopy analysis of biofilm growth

Bacteria and *C. albicans* were cultured in 96-well polystyrene plates (SPL Life Sciences, Korea) with or without CGNPs. Planktonic cells were then removed by washing with PBS buffer and stained with carboxyfluorescein diacetate succinimidyl ester (Invitrogen, Molecular probes Inc., Eugene, USA). Biofilms were visualized under a Nikon Eclipse Ti (Tokyo) confocal laser scanning microscope (CLSM) equipped with a 20× objective. Three-dimensional biofilm color images were constructed using NIS-Elements C version 3.2 (Nikon eclipse). At least 10 random positions were chosen each of two independent cultures.

2.7. Visualization of hyphal inhibition

The inhibitory effect of CGNPs on the yeast-to-hypha transition was determined using RPMI 1640 (Invitrogen, USA) medium buffered with HEPES (pH 7.3) after treatment for 24 h at 37 °C. Samples were withdrawn at predetermined times and the impact of CGNPs on hyphal growth was visualized using the iRiS™ Digital Cell Imaging System (Logos Biosystems, Anyang, Korea) equipped with an inverted Plan Achromatic 20× or 40× Ph objective lens.

2.8. Morphological analysis of C. albicans with CGNPs

To evaluate possible surface interactions caused by CGNPs on *C. albicans*, cells were treated and analyzed by transmission electron microscopy (TEM). Initially, overnight grown cells were incubated with CGNPs at 0.007% v/v for 24 h with shaking at 37 °C. Pre-fixation was performed using aldehyde mixture (glutaraldehyde 2.5% and formaldehyde 2%) and the cells were harvested by using centrifugation, washed with water and immediately post-fixed using 2% osmium tetroxide and kept overnight at 4 °C. 0.2 M phosphate buffer was used to wash the cells and cell blocks were made using 2% agarose. After dehydration with series of ethanol, the specimens were embedded in an Epon resin (Hatfield, USA), which was kept at different temperatures for complete polymerization. Thin sections were made using a MT-X ultramicrotome (Tucson, USA) and loaded onto TEM grids. The grids were stained with 1% uranyl acetate followed by lead citrate in the presence of sodium hydroxide. Finally, microscopy was performed using a H-7600 electron microscope (Tokyo, Japan) at 120-keV.

3. Results and discussion

3.1. Synthesis and characterizations of CGNPs

In this study, cinnamaldehyde was used as a reducing agent at 100 °C to prepare CGNPs in one-step. The formation of CGNPs was visualized by a color change from pale yellow to pinkish-purple (Fig. 1a inset) within a minute of mixing indicating reduction of Au^{3+} to Au (0). When alcohols (ethanol) added to aldehydes, it reacted and formed reversible hemiacetal or acetal. But in the presence of excess water or aqueous acid, the formed hemiacetal or acetal may be hydrolyzed back into their starting components of aldehydes or ketones. Additionally, elsewhere available references [21–23] explain that the —CHO group's involvement and the importance of heat in the metal ion reduction processes to produce nanoparticles.

UV–vis spectroscopy provides an indirect means of examining the production of CGNPs from gold chloride solution because it detects the surface plasmon resonance (SPR) of metallic nanoparticles, which is related to nanoparticle size, shape, interparticle distances, and the surrounding environment [24]. Fig. 1a shows the narrow peak at 540 nm emanating from small spherical GNPs. CGNPs also exhibited an absorption band at 290 nm that exactly matched a peak in reference spectrum of cinnamaldehyde [25], and confirmed its involvement in the reduction process. Further, the appearance of two well resolved bands in the SPR's of CGNPs provided direct evidence of the formation of stable CGNP complexes in aqueous solution. At the same time, cinnamaldehyde having 290 nm as maximum UV absorbance could be due to the extended π-conjugation with benzene ring. In corroboration, the produced cinnamaldehyde immobilized gold nanoparticles (Figs. 1 and 2 and S1) showed the absorption spectra at 290 nm which belongs to cinnamaldehyde thus confirming the production of cinnamaldehyde-metal core complex. For a comparison, we prepared nanoparticles using cinnamic acid which showed maximum absorbances at 260 nm [26,27] and 554 nm for cinnamic acid and GNPs, respectively. Also, cinnamic acid utilized >16 min (data not shown) to reduce metal salts to form nanoparticles which is much longer than cinnamaldehyde mediated synthesis. At the same time cinnamic acid produced nanoparticles suffered with low UV–vis absorption intensity at 554 nm with broad spectra (Fig. S1) corre-

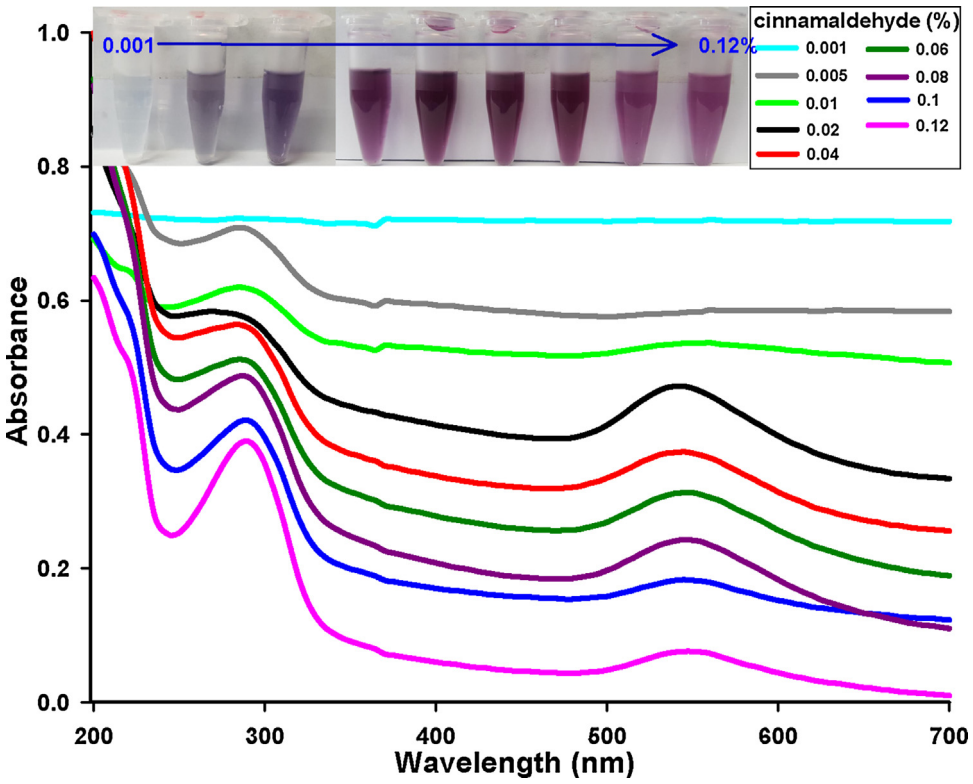

Fig. 2. The impact of cinnamaldehyde concentration on CGNP formation. Different concentrations (0.001–0.12%) were examined to assess the reducing power of cinnamaldehyde. The inset shows color changes (indicative of CGNP formation) observed on increasing cinnamaldehyde concentration.

sponding to the formation of larger nanoparticles. These results confirmed that cinnamaldehyde is a better and major reducing agent to produce uniformly sized GNPs than cinnamic acid.

TEM was used to determine the shape, dimensions, and distributions of CGNPs (Fig. 1b). The CGNPs produced were spherical, had a narrow size distribution (11 ± 3 nm), and exhibited a high degree of crystallinity. In addition to acting as a reducing agent cinnamaldehyde capped GNPs to provide resistance to aggregation. Hence, contrast differences in the metal core and surface covering from the magnified view of Fig. 1b inset revealed the formation of CGNP complexes with distinct interfacial and spatial arrangements between nanostructures [28–30].

The reaction between cinnamaldehyde and Au ions was confirmed by ATR-FTIR spectroscopy (Fig. S2). cinnamaldehyde displayed characteristic peaks at 1680 cm^{-1} and 1621 cm^{-1} corresponded to the stretching vibrations of C=O and C=C groups [31,32]. The presence of signature peaks at 1718 cm^{-1} and 1650 cm^{-1} indicating cinnamaldehyde/GNP complex formation. The disappearance of peak at 1125 cm^{-1} after reaction showed −CHO was mainly responsible for reducing Au ions. Furthermore, CGNPs exhibited distinctive peaks at 638, 803, and 1380 cm^{-1} corresponding to (CH=CH bending, —CH bending, and —CH stretching, respectively) of the phenyl group of cinnamaldehyde. The two characteristic signatures at 1508 and 1088 cm^{-1} were assigned to —C—O—C— or —C—O—, derived from heterocyclic alkaloids which cap nanoparticles [33].

3.2. Optimization of CGNPs synthesis

To ascertain the role of reducing agent involvement in the production of CGNPs, cinnamaldehyde concentration was optimized by UV–vis spectrophotometry. Increasing the concentration of cinnamaldehyde resulted in a SPR red-shift. As shown in Fig. 2, at concentrations less than (0.02%) no CGNPs were formed but at concentrations between 0.02–0.12% showed distinct peaks claiming the formation of CGNPs. Depending on varying cinnamaldehyde concentrations, the CGNPs formation was differed which exhibited color changes (Fig. 2 inset). Appearance of intense pinkish violet color indicates the formation of stable CGNPs (at 0.02–0.06% of cinnamaldehyde) which showed better absorbance intensity. On the other hand, blue color at lower cinnamaldehyde concentration (0.005 and 0.01%) and less intense pinkish violet color appeared at highest cinnamaldehyde concentrations (0.1 and 0.12%) showed that there was no nanoparticle formation or increasing cinnamaldehyde concentration could not efficiently reduce Au ion into nanoparticles, respectively. Further, it was noted from DLS measurements that larger particles at 190 ± 32 nm (data not shown) were obtained at cinnamaldehyde concentration of 0.12% and smaller particles (114 ± 21 nm) (Table S1) were produced at 0.02% concentration. According to the results obtained a cinnamaldehyde concentration of 0.02% was considered optimal in terms of producing smaller particles. Since, chemicals of greater reducing capacity are more effective at reducing metallic ions to nanoparticles [34,35], we believe cinnamaldehyde could acted as reducing agent by neutralizing free radicals to form CGNPs [36–38]. Thus, it would appear nanoparticles produced using cinnamaldehyde could prevent or reduce the harmful effects of reactive oxygen species [39].

Fig. 3 shows a histogram of CGNP polydispersity index (PDI) versus Au distribution. Initially, PDI of CGNPs decreased as Au^{3+} concentration increased from 20 to 100 μM and remained low (between 0.06 and 0.08) for concentrations up to 140 μM. Also, for more concentrated Au solutions (up to 200 μM), higher PDI values were obtained indicating the formation of asymmetric particles or larger aggregates. At Au^{3+} concentrations between 100 and 140 μM highly mono-dispersed particles were formed, and thus, 120 μM was determined to be the optimum Au^{3+} concentration range for nanoparticle formation. Furthermore, the absorption intensities of

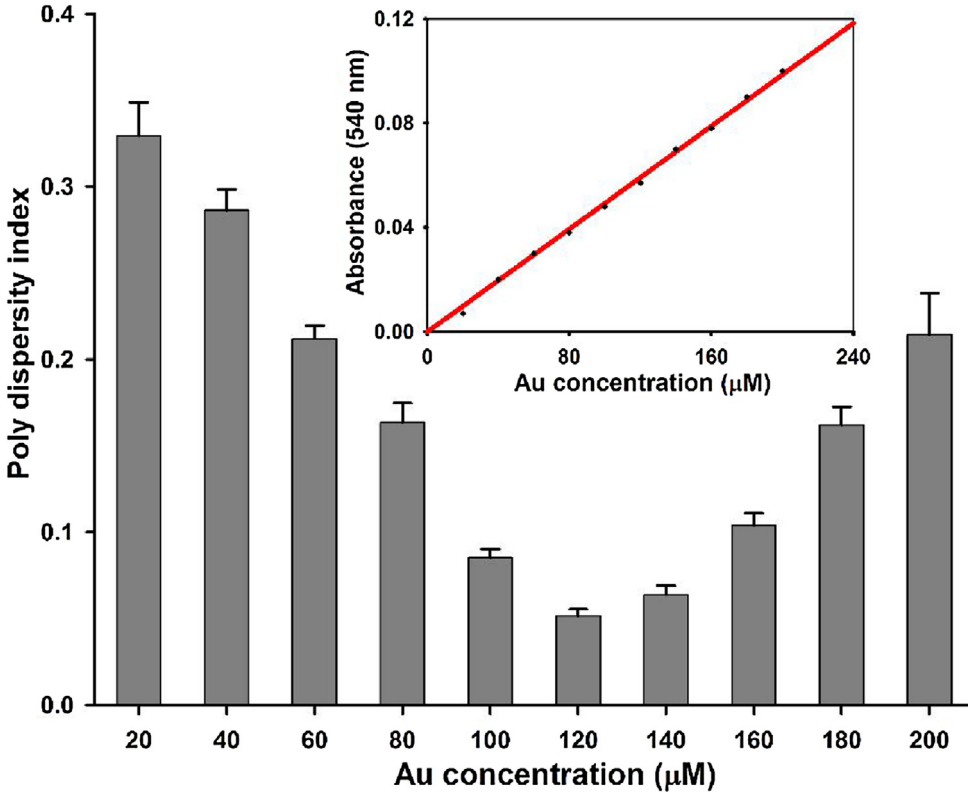

Fig. 3. Influence of Au concentration on CGNP's poly dispersity index of particle size distributions. The inset shows the linear relation between CGNP absorbance and Au concentrations.

the CGNPs produced at 540 nm were found to be linearly related to Au^{3+} concentration, showing that nanoparticle synthesis obeyed the Beer-Lambert law (Fig. 3 inset). These results show it is possible to generate concentrated solutions of monodisperse CGNPs by choosing the appropriate concentration of Au [40].

The influence of pH's (3, 7 and 11) at different temperatures (25 or 100 °C) was investigated on nanoparticle complex formation by cinnamaldehyde for different metal salts ($AgNO_3$, $CuSO_4$, TiO_2, and Zn $(NO_3)_2$) (Fig. 4a). Since changes in reaction mixture colors are indicative of nanoparticle formation [41], the color changes produced were photographed. As shown in Fig. 4a, cinnamaldehyde reduced Au, Ag, Ti, and Zn under specific temperatures and pH values. For Au, particle formation was observed at all pH values excepting pH 3 and 7 at 25 °C. Ag was reduced by cinnamaldehyde to form silver nanoparticles in pH 3 and 11 at 100 °C, but no color change under other conditions. For Cu no color was observed under any experimental condition. On the other hand, cinnamaldehyde reduced Ti and Zn, which produced a mild white color at pH values of 7 and 11 at 25 °C. Furthermore, observed color changes correlated with UV–vis spectrophotometry absorbance spectra. When reduced by cinnamaldehyde, Au, Ag Ti, and Zn (Fig. S3a–S3d) showed specific plasmon resonance absorptions at 430, 540, 454, and 365 nm, respectively, which confirmed nano-particle formations [42–45]. These experiments showed cinnamaldehyde can act as a powerful reducing agent and reduce Au, Ag, Ti, and Zn to form their respective nanoparticles. As previously reported, phytochemicals with high antioxidant and reducing powers efficiently generate nanoparticles [34,35], and as shown by the present study, cinnamaldehyde is a strong enough reducing agent to synthesize a wide variety of metal nanoparticles in a single-stage process.

Different light sources were used to examine the effect of light on CGNP formation; particle sizes were determined by DLS. As illustrated in the figure (Fig. 4b), the reduction of Au ions to CGNPs, as evidenced by color change to pinkish-purple, was observed when reaction mixtures were exposed to different light sources or even left in the dark. However, no color change was observed when the reaction was attempted at 4 °C in the dark. Thus, although light promoted nanoparticle production, heat would seem to play a predominant role. This result (Table S1) concurs with a previous report [46] that temperature was largely responsible for the formation of smaller nanoparticles. In addition, the CGNPs produced had similar PDI values and high zeta potential values indicating high stability. Hence, cinnamaldehyde with or without light formed stable nanoparticles at higher temperatures.

3.3. Antimicrobial activity against pathogens

The antimicrobial activities of cinnamaldehyde, CGNPs, cinnamic acid, GNPs, SiGNPs and TGNPs were investigated by measuring MICs. For the tested bacteria and *C. albicans*, the MICs of CGNPs were found to range from 0.008 to 0.05% (Table S2). Notably, cinnamaldehyde requires higher concentrations (almost 2-fold high) than CGNPs to suppress the microbial growth for all the tested strains. Meantime, cinnamic acid, GNPs, SiGNPs and TGNPs have showed high MICs of >0.1%, claiming no antimicrobial activity. These results confirmed that CGNPs effectively involved in microbicidal activity which was in corroboration with antibiofilm activity. This study explained that regardless of microbial cell's nature, all the tested microorganisms were susceptible to CGNPs because the smaller sized CGNPs get attached to microorganisms due to the liphophilic attraction between cinnamaldehyde (present in CGNPs) and microbial cell wall [47].

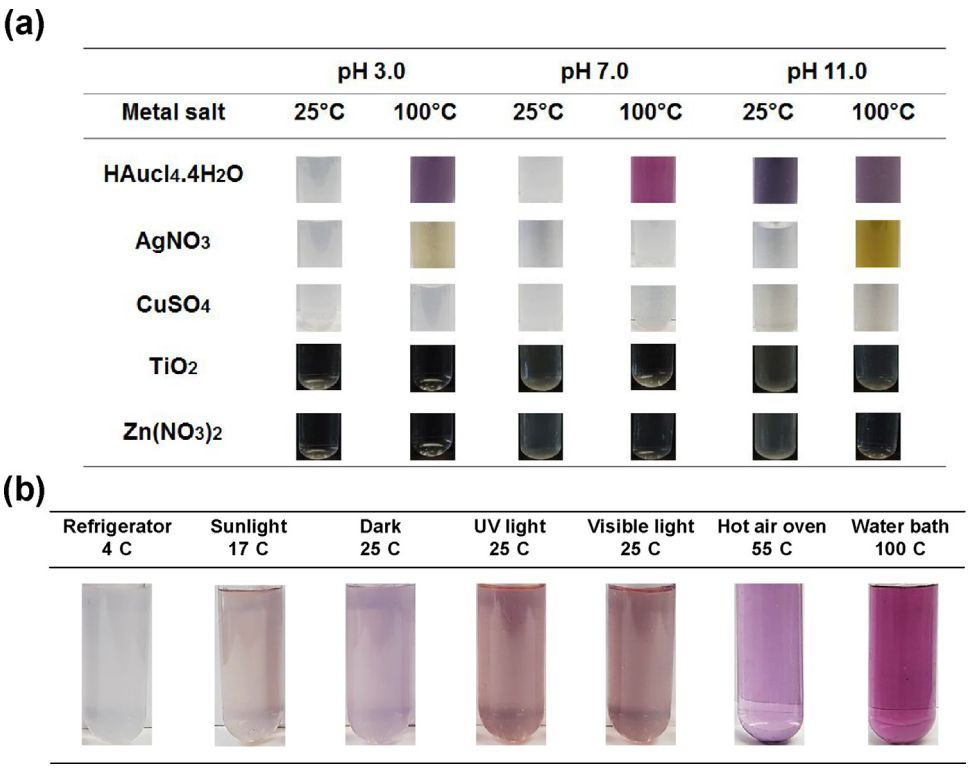

Fig. 4. Influences of pH and temperature on the one-pot synthesis of various metal nanoparticles (a), and effects of different light sources on the synthesis of CGNPs at varying temperatures (b).

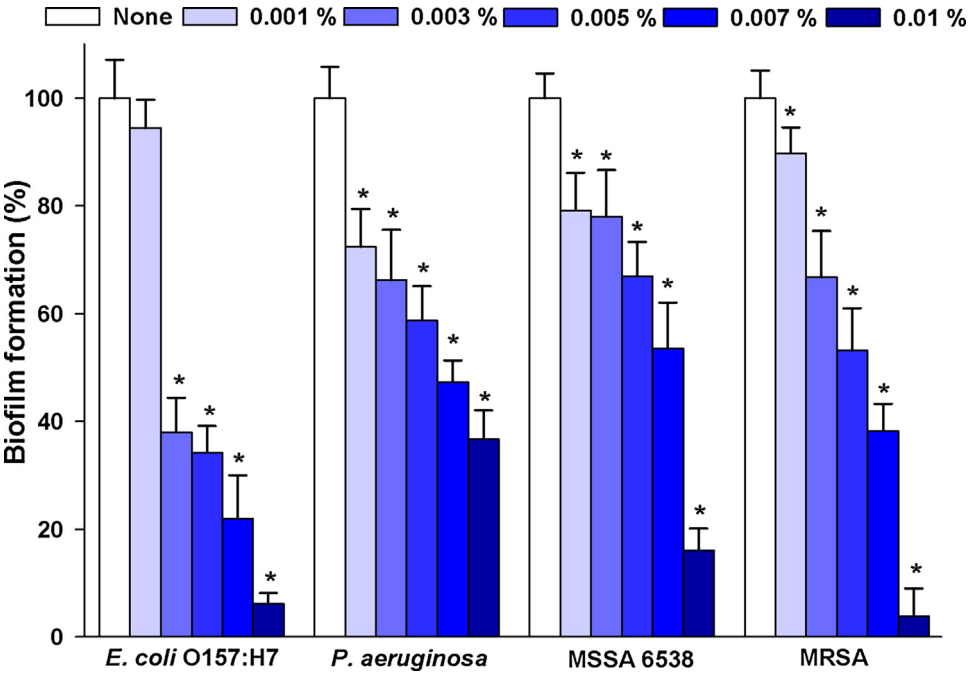

Fig. 5. The effects of CGNPs on biofilm formation by *E. coli* O157:H7, *P. aeruginosa*, MSSA 6538, and MRSA were examined after incubation for 24 h in 96-well plates without shaking. $^{*}p < 0.05$ versus control.

3.4. Inhibition of biofilm growth and development

The inhibitory effects of CGNPs at 0-0.01% on biofilm formations by *E. coli* O157:H7, *P. aeruginosa*, MSSA 6538, MRSA, and *C. albicans* were investigated using static biofilm assay (Fig. 5 and Fig. 6a, b). All tested strains showed significant dose-dependent antibiofilm effects that agreed well with MICs values. At a concentration of 0.01%, CGNPs inhibited biofilm formation by *E. coli* O157:H7 and MRSA by >90%, and biofilm formation by *P. aeruginosa* and MSSA 6538 by ~65% and >85%, respectively. *P. aeruginosa* biofilms were more resistant than those of the other bacteria, which may have been due to the ability of this bacterium to change its outer membrane after interacting with CGNPs [48]. Of the microorganisms tested, *C. albicans* biofilm growth was inhibited by ~93% by CGNPs

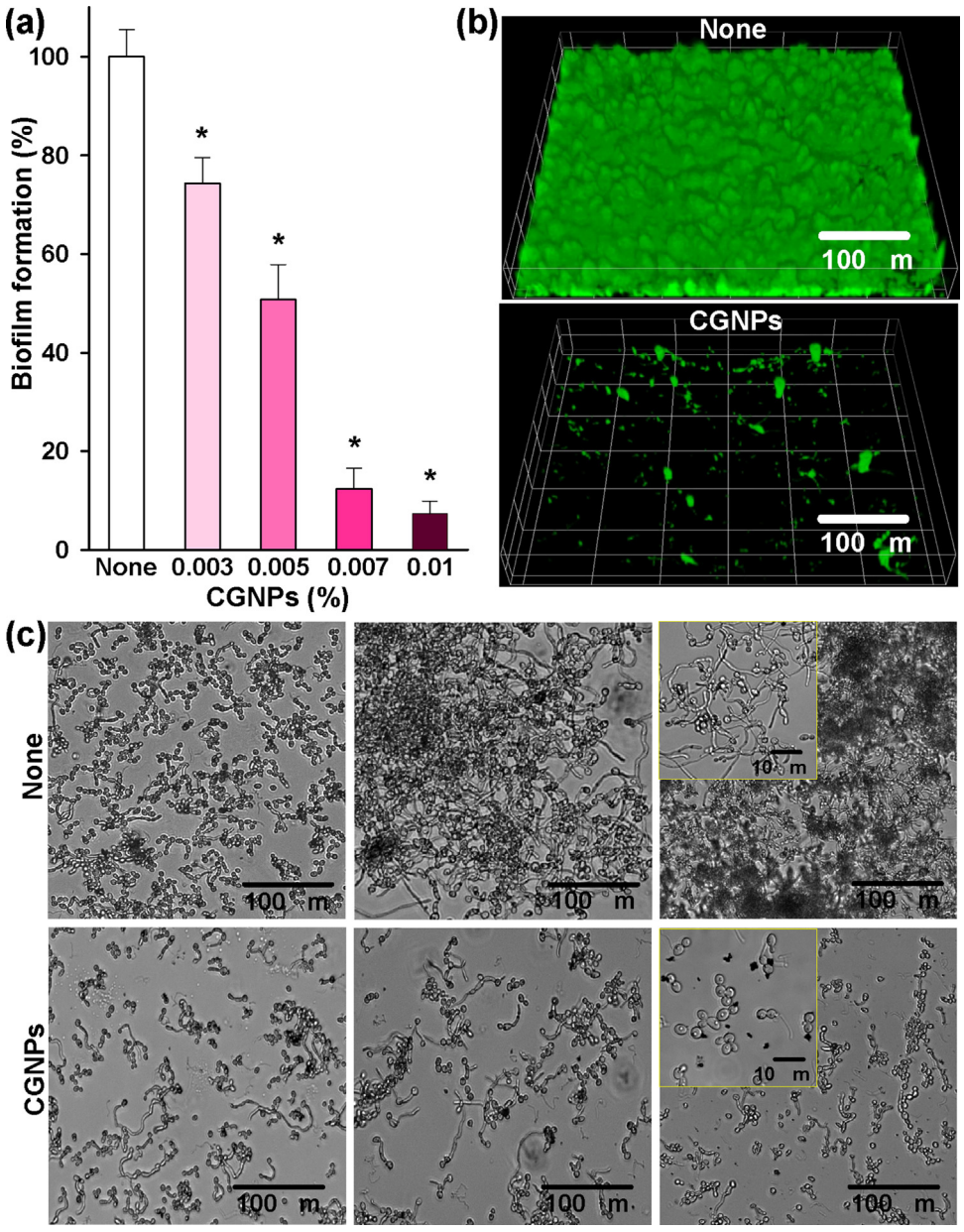

Fig. 6. Antifungal activity of CGNPs. The effects of different concentrations of CGNPs, on biofilm formation by *C. albicans* (a), confocal laser photomicrograph showing structural alterations in biofilms treated with CGNPs at 0.01% (b) optical photomicrographs of hyphal inhibition by CGNPs after treatment for different times (c). 'None' indicates no CGNP treatment.

at 0.01%, which also inhibited *E. coli* O157:H7, *P. aeruginosa*, MSSA 6538, and MRSA growth by >50% (Fig. S4). Surprisingly, *C. albicans* cell growth was completely inhibited by CGNPs at 0.01% (data not shown). To corroborate antibiofilm results, we examined structural changes in *C. albicans* biofilms using confocal microscope (Fig. 6b). As compared to untreated controls, biofilm formation was inhibited by >90% by CGNPs at 0.01%. These observations suggest CGNPs might permeate biofilm layers and eradicate sessile bacteria due to the presence of cinnamaldehyde.

Additionally, impacts of bare GNPs, and surface modified GNPs including SiGNPs, and TGNPs on pathogenic biofilms at 0-0.01%, w/v concentrations were investigated against pathogenic strains of *E.coli* O157:H7, MSSA 6538 and *C. albicans* (Fig. S5). At the tested concentrations, GNPs, SiGNPs, and TGNPs showed no significant antibiofilm activity (Fig. S5) on all three microbes. In contrast, CGNPs effectively inhibited biofilm formation by bacteria and a fungi (Figs. 5 and 6). This specific antibiofilm activity of CGNPs could due to the penetration of deeper biofilm layers and eradicate sessile bacteria after exposure to attached cinnamaldehyde. Henceforth, the unavailability of antimicrobial agent like cinnamaldehyde in bare and ligand attached GNPs showed no antibiofilm activity rather promoting the cell growth which might be due to the non-toxic nature of surface ligands including silica and tyrosine [49–52]. On the other hand, the effects of cinnamaldehyde reduced silver nanoparticles (CAgNPs) on biofilm formation was assessed using *E. coli* O157:H7, MSSA 6538, and *C. albicans*. Without a wonder, a remarkable biofilm inhibition on all the strains (Fig. S6) were observed which might be due to the synergistic antimicrobial activity of cinnamaldehyde with silver nanoparticles [53]. However, after considering the utilization of high pH values by $AgNO_3$ to form CAgNPs that requires longer processing steps to make it biocompatible and because of harmful toxic nature of silver ions from AgNPs [54–56], further applications of CAgNPs in our experiments was limited.

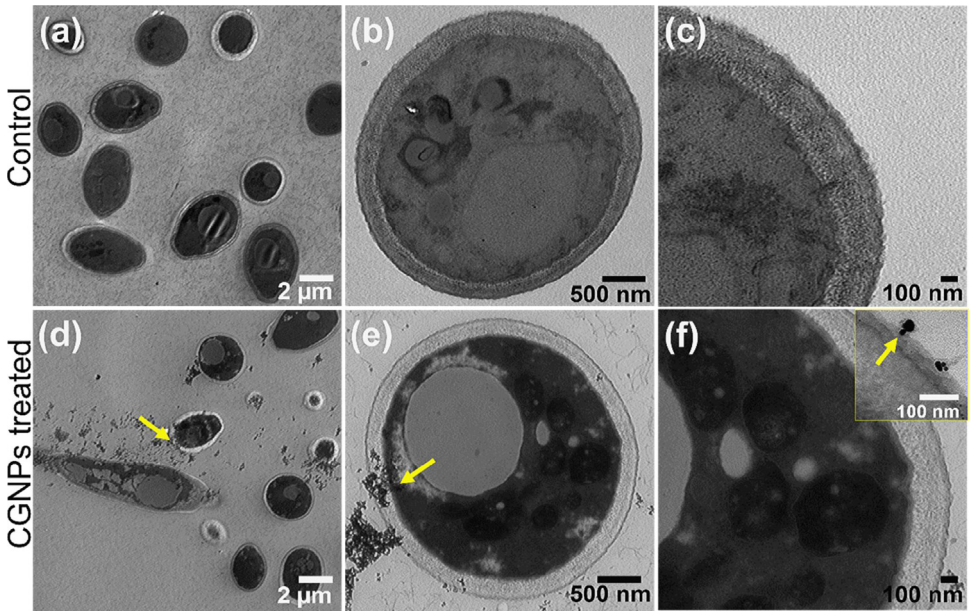

Fig. 7. Transmission electron microscopy (TEM) of untreated and CCGNPs treated *C. albicans*. Control cells show regular contour cytoplasm (a and b) and the magnified view show intact cell structure without any damage (c). Treated cells show the entry of CGNPs through cell wall (d and e) and severe intracellular damage (f). Yellow arrows indicate the presence of CGNPs and the inset displays CGNPs attachment on the cell membrane of *C. albicans* (f inset). (For interpretation of the references to colour in this figure legend, the reader is referred to the web version of this article.)

3.5. *Biological activity of CGNPs on* C. albicans *yeast-to-hypha transition*

Recognizing the positive link between biofilms and hyphal development in *C. albicans*, the effects of CGNPs on yeast-to-hyphal transitions were tested [57]. Optical microscopy (iRiS^{TM} Digital Cell Imaging System) was utilized to examine the degree of hyphal inhibition by CGNPs at 0.01%, which was previously found to reduce biofilm formation effectively by crystal violet staining after 24 h of incubation (Fig. 6c). In untreated samples, culture in PDB for 4–48 h caused the fungi to produce pseudohyphae and true hyphal formation up to the characteristic filamentous hyphal stage. In contrast, in the presence of CGNPs 0.01%, hyphal formation was inhibited from 4 h, and at 48 h, only fungal cells without hyphae were observed. One plausible mechanism of this effect on hyphal formation is that CGNPs inactivate hydrolytic enzymes in the fungi thus reduced virulence by hyphal inhibition [58].

3.6. *Interactions of CGNPs with C. albicans*

To understand the surface interactions of CGNPs to a biological system, a cross-sectional TEM on CGNPs treated *C. albicans* was performed (Fig. 7). Untreated control cells retained a normal morphology with intact thin cell walls and cytoplasm (Fig. 7a and b) [59]. Magnified view (Fig. 7c) depicts visible organelles in the cytoplasm and mitochondria with intact plasma membrane. On the other hand, prominent changes were observed in CGNPs treated *C. albicans* including degraded cytoplasm, destroyed organelles and many necrotic cells (Fig. 7d and e) [47,60]. Importantly, attachment and entry of CGNPs through cell walls clearly visible from Fig. 7f inset, indicating that CGNPs penetrated through cell wall and caused severe damage to the cytoplasm and significant morphological changes including storage granules and disintegration of intracellular structures. Hence, we suggest that the diminutive sized CGNPs could penetrate cell wall, interacted with intracellular components, released cinnamaldehyde and destroyed the *C. albicans* cells.

To the best of our knowledge, this is the first report to describe a simple, one-pot synthesis of water dispersible CGNP nanocomplexes with enhanced antimicrobial/antibiofilm properties. Although in a previous report, we found that the anti-biofilm effect of cinnamaldehyde coated GNPs required additional chemicals and extra processing times to ensure nanoparticles were well coated to achieve intended activity [42]. The method used in the present study allows CGNPs to be produced in a single step with no additional reagents. In other studies considerably higher concentrations of cinnamaldehyde (up to 5%, v/v) were used to achieve antimicrobial activity [32,48].

Since the exact mechanism of action of CGNPs is not fully understood, we propose the hypothesis that because of ultrasmall size and large surface area CGNPs could permeate through biofilms and causing antimicrobial/antibiofilm activity. Even though free cinnamaldehyde is lipophilic, it could not pass through biofilm layers but CGNPs could invade those layers and might delivered cinnamaldehyde to eradicate sessile bacteria. As reported earlier [61,62], the current study suggests that the diminutive sizes of CGNPs are responsible for the penetration through biofilm layers, reach cells, interact with cellular components and kill microbes. Furthermore, the acidic pH of biofilm could hydrolyze CGNPs and release cinnamaldehyde to exert antimicrobial activity [63,64]. Furthermore, we believe that cinnamaldehyde in nanocomplexes may disrupts cytoplasmic contents [65], inhibits quorum sensing [66], penetrates cell walls due to its lipophilic nature [47], and induces protein release or precipitation [67]. The antimicrobial and antibiofilm properties of CGNPs observed on pathogenic, multi-drug resistant bacteria, and *C. albicans* suggests that cinnamaldehyde containing CGNP nanocomplexes offers a potential alternative to traditional antibiotics.

4. Conclusions

In summary, we used cinnamaldehyde to produce metal nanoparticles in an eco-friendly manner. We found that reaction conditions significantly influenced nanoparticle production, and that their optimization resulted in a one-pot method of rapidly

producing stable, mono-dispersed CGNPs. Furthermore, CGNPs effectively inhibited pathogenic fungal and bacterial biofilms, which may reduce antibiotic resistance. Our observations suggest that cinnamaldehyde offers a means of avoiding the use of toxic chemicals to make potentially therapeutic metal nanoparticles in a single-step.

Disclosure

The authors have no conflict of interest to declare.

Acknowledgements

This research was supported by the National Research Foundation of Korea (NRF) funded by the Korean government (MSIP) (#2015R1A2A2A01004542 to J. Lee) and by the Priority Research Center Program through the NRF funded by the Ministry of Education (#2014R1A6A1031189).

Appendix A. Supplementary data

Supplementary data associated with this article can be found, in the online version, at https://doi.org/10.1016/j.colsurfb.2017.10.018.

References

[1] K. Vasilev, V. Sah, K. Anselme, C. Ndi, M. Mateescu, B.r. Dollmann, P. Martinek, H. Ys, L. Ploux, H.J. Griesser, Tunable antibacterial coatings that support mammalian cell growth, Nano Lett. 10 (2009) 202–207.
[2] W.H. Organization, Antimicrobial Resistance Global Report on Surveillance, World Health Organization, 2014, pp. 257.
[3] A.Y. Peleg, D.C. Hooper, Hospital-acquired infections due to gram-negative bacteria, N. Engl. J. Med. 362 (2010) 1804–1813.
[4] Y. Zhan, W. Zeng, G. Jiang, Q. Wang, X. Shi, Z. Zhou, H. Deng, Y. Du, Construction of lysozyme exfoliated rectorite-based electrospun nanofibrous membranes for bacterial inhibition, J. Appl. Polym. Sci. 132 (2015).
[5] D. Davies, Understanding biofilm resistance to antibacterial agents, Nat. Rev. Drug. Discov. 2 (2003) 114–122.
[6] L.R. Hoffman, D.A. D'Argenio, M.J. MacCoss, Z. Zhang, R.A. Jones, S.I. Miller, Aminoglycoside antibiotics induce bacterial biofilm formation, Nature 436 (2005) 1171–1175.
[7] U. Ikoba, H. Peng, H. Li, C. Miller, C. Yu, Q. Wang, Nanocarriers in therapy of infectious and inflammatory diseases, Nanoscale 7 (2015) 4291–4305.
[8] C.J. Murphy, T.K. Sau, A.M. Gole, C.J. Orendorff, J. Gao, L. Gou, S.E. Hunyadi, T. Li, Anisotropic metal nanoparticles: synthesis, assembly, and optical applications, J. Phys. Chem. B 109 (2005) 13857–13870.
[9] D.K. Yi, I.-C. Sun, J.H. Ryu, H. Koo, C.W. Park, I.-C. Youn, K. Choi, I.C. Kwon, K. Kim, C.-H. Ahn, Matrix metalloproteinase sensitive gold nanorod for simultaneous bioimaging and photothermal therapy of cancer, Bioconjug. Chem. 21 (2010) 2173–2177.
[10] W. Li, X. Li, Q. Wang, Y. Pan, T. Wang, H. Wang, R. Song, H. Deng, Antibacterial activity of nanofibrous mats coated with lysozyme-layered silicate composites via electrospraying, Carbohydr. Polym. 99 (2014) 218–225.
[11] S. Iravani, Green synthesis of metal nanoparticles using plants, Green Chem. 13 (2011) 2638–2650.
[12] N. Khlebtsov, L. Dykman, Biodistribution and toxicity of engineered gold nanoparticles: a review of in vitro and in vivo studies, Chem. Soc. Rev. 40 (2011) 1647–1671.
[13] Z. Bao, Y. Yuan, C. Leng, L. Li, K. Zhao, Z. Sun, One-pot synthesis of noble metal/zinc oxide composites with controllable morphology and high catalytic performance, ACS Appl. Mater. Interfaces 9 (2017) 16417–16425.
[14] T.B. Adams, S.M. Cohen, J. Doull, V.J. Feron, J.I. Goodman, L.J. Marnett, I.C. Munro, P.S. Portoghese, R.L. Smith, W.J. Waddell, The FEMA GRAS assessment of cinnamyl derivatives used as flavor ingredients, Food. Chem. Toxicol. 42 (2004) 157–185.
[15] H. Li, Q. Shen, W. Zhou, H. Mo, D. Pan, L. Hu, Nanocapsular dispersion of cinnamaldehyde for enhanced inhibitory activity against aflatoxin production by *Aspergillus flavus*, Molecules 20 (2015) 6022–6032.
[16] H. Chen, P.M. Davidson, Q. Zhong, Impacts of sample preparation methods on solubility and antilisterial characteristics of essential oil components in milk, Appl. Environ. Microbiol. 80 (2014) 907–916.
[17] C. Bilbao-Sainz, B.-S. Chiou, W.-X. Du, K.S. Gregorsky, W.J. Orts, Influence of disperse phase characteristics on stability, physical and antimicrobial properties of emulsions containing cinnamaldehyde, J. Am. Oil Chem. Soc. 90 (2013) 233–241.
[18] C. Gomes, R.G. Moreira, E. Castell-Perez, Poly (DL-lactide-co-glycolide)(PLGA) nanoparticles with entrapped trans-cinnamaldehyde and eugenol for antimicrobial delivery applications, J. Food Sci. 76 (2011) N16–N24.
[19] M.F. Canbolat, A. Celebioglu, T. Uyar, Drug delivery system based on cyclodextrin-naproxen inclusion complex incorporated in electrospun polycaprolactone nanofibers, Colloids Surf. B Biointerfaces 115 (2014) 15–21.
[20] J.H. Lee, M.H. Cho, J. Lee, 3-Indolylacetonitrile decreases *Escherichia coli* O157:H7 biofilm formation and *Pseudomonas aeruginosa* virulence, Environ. Microbiol. 13 (2011) 62–73.
[21] N. Vigneshwaran, R.P. Nachane, R.H. Balasubramanya, P.V. Varadarajan, A novel one-pot 'green' synthesis of stable silver nanoparticles using soluble starch, Carbohydr. Res. 341 (2006) 2012–2018.
[22] J.F. Gomes, A.C. Garcia, E.B. Ferreira, C. Pires, V.L. Oliveira, G. Tremiliosi-Filho, L.H. Gasparotto, New insights into the formation mechanism of Ag, Au and AgAu nanoparticles in aqueous alkaline media: alkoxides from alcohols, aldehydes and ketones as universal reducing agents, Phys. Chem. Chem. Phys. 17 (2015) 21683–21693.
[23] V. Makarov, A. Love, O. Sinitsyna, S. Makarova, I. Yaminsky, M. Taliansky, N. Kalinina, Green nanotechnologies: synthesis of metal nanoparticles using plants, Acta Naturae 6 (2014) 35–44.
[24] A. Moores, F. Goettmann, The plasmon band in noble metal nanoparticles: an introduction to theory and applications, New J. Chem. 30 (2006) 1121–1132.
[25] D. Kalemba, A. Kunicka, Antibacterial and antifungal properties of essential oils, Curr. Med. Chem. 10 (2003) 813–829.
[26] G.S. Hu, J.M. Jia, Y.J. Hur, Y.S. Chung, J.H. Lee, D.J. Yun, W.S. Chung, G.H. Yi, T.H. Kim, D.H. Kim, Molecular characterization of phenylalanine ammonia lyase gene from *Cistanche deserticola*, Mol. Biol. Rep. 38 (2011) 3741–3750.
[27] H. Zhang, J.-C. Kim, Doxorubicin-loaded microgels composed of cinnamic acid–gelatin conjugate and cinnamic acid–Pluronic F127 conjugate, Pharm. Dev. Technol. 21 (2016) 296–301.
[28] K.V. Katti, R. Kannan, K.K. Katti, S.K. Nune, Stabilized, biocompatible gold nanoparticles, Google Patents, 2014.
[29] J. Lee, H.Y. Kim, H. Zhou, S. Hwang, K. Koh, D.-W. Han, J. Lee, Green synthesis of phytochemical-stabilized Au nanoparticles under ambient conditions and their biocompatibility and antioxidative activity, J. Mater. Chem. 21 (2011) 13316–13326.
[30] Z.E.J. Pérez, R. Mathiyalagan, J. Markus, Y.-J. Kim, H.M. Kang, R. Abbai, K.H. Seo, D. Wang, V. Soshnikova, D.C. Yang, Ginseng-berry-mediated gold and silver nanoparticle synthesis and evaluation of their in vitro antioxidant, antimicrobial, and cytotoxicity effects on human dermal fibroblast and murine melanoma skin cell lines, Int. J. Nanomed. 12 (2017) 709.
[31] Z. Tian, X. Xiang, L. Xie, F. Li, Liquid-phase hydrogenation of cinnamaldehyde: enhancing selectivity of supported gold catalysts by incorporation of cerium into the support, Ind. Eng. Chem. Res. 52 (2012) 288–296.
[32] B. Duncan, X. Li, R.F. Landis, S.T. Kim, A. Gupta, L.-S. Wang, R. Ramanathan, R. Tang, J.A. Boerth, V.M. Rotello, Nanoparticle-stabilized capsules for the treatment of bacterial biofilms, ACS Nano 9 (2015) 7775–7782.
[33] J. Huang, Q. Li, D. Sun, Y. Lu, Y. Su, X. Yang, H. Wang, Y. Wang, W. Shao, N. He, Biosynthesis of silver and gold nanoparticles by novel sundried Cinnamomum camphora leaf, Nanotechnology 18 (2007) 105104.
[34] A. Wojdyło, J. Oszmiański, R. Czemerys, Antioxidant activity and phenolic compounds in 32 selected herbs, Food Chem. 105 (2007) 940–949.
[35] D. Ştef, I. Gergen, T. Traşcă, L. Ş. Monica Hărmănescu, B. Ramone, M. Heghedus, Total antioxidant and radical scavenging capacities for different medicinal herbs, Rom. Biotechnol. Lett. 14 (2009) 4705–4710.
[36] M.P. Kähkönen, A.I. Hopia, H.J. Vuorela, J.-P. Rauha, K. Pihlaja, T.S. Kujala, M. Heinonen, Antioxidant activity of plant extracts containing phenolic compounds, J. Agric. Food Chem. 47 (1999) 3954–3962.
[37] C.A. Rice-evans, N.J. Miller, P.G. Bolwell, P.M. Bramley, J.B. Pridham, The relative antioxidant activities of plant-derived polyphenolic flavonoids, Free Radic. Res. 22 (1995) 375–383.
[38] B. Zheng, X. Jing, T. Odoom-Wubah, T. Kong, H. Chen, D. Sun, J. Huang, Q. Li, Catalytic application of biogenic platinum nanoparticles for the hydrogenation of cinnamaldehyde to cinnamyl alcohol, Synth. React. Inorg. Met. Org. Chem. 45 (2015) 967–973.
[39] T. Karuppanapandian, J.-C. Moon, C. Kim, K. Manoharan, W. Kim, Reactive oxygen species in plants: their generation, signal transduction, and scavenging mechanisms, Aust. J. Crop. Sci 5 (2011) 709.
[40] K. Zabetakis, W.E. Ghann, S. Kumar, M.-C. Daniel, Effect of high gold salt concentrations on the size and polydispersity of gold nanoparticles prepared by an extended Turkevich–Frens method, Gold Bull. 45 (2012) 203–211.
[41] H.-s Kim, Y.S. Seo, K. Kim, J.W. Han, Y. Park, S. Cho, Concentration effect of reducing agents on green synthesis of gold nanoparticles: size, morphology, and growth mechanism, Nanoscale Res. Lett. 11 (2016) 230.
[42] M. Ramasamy, J.-H. Lee, J. Lee, Development of gold nanoparticles coated with silica containing the antibiofilm drug cinnamaldehyde and their effects on pathogenic bacteria, Int. J. Nanomed. 12 (2017) 2813.
[43] G. Goyal, J. Hwang, J. Aviral, Y. Seo, Y. Jo, J. Son, J. Choi, Green synthesis of silver nanoparticles using β-glucan, and their incorporation into doxorubicin-loaded water-in-oil nanoemulsions for antitumor and antibacterial applications, Ind. Eng. Chem. 47 (2017) 179–186.
[44] M.M. Khan, S.A. Ansari, D. Pradhan, M.O. Ansari, J. Lee, M.H. Cho, Band gap engineered TiO 2 nanoparticles for visible light induced photoelectrochemical and photocatalytic studies, J. Mater. Chem. A Mater. Energy Sustain. 2 (2014) 637–644.

[45] P. Fageria, S. Gangopadhyay, S. Pande, Synthesis of ZnO/Au and ZnO/Ag nanoparticles and their photocatalytic application using UV and visible light, RSC Adv. 4 (2014) 24962–24972.
[46] G. Mountrichas, S. Pispas, E.I. Kamitsos, Effect of temperature on the direct synthesis of gold nanoparticles mediated by poly(dimethylaminoethyl methacrylate) homopolymer, J. Phys. Chem. C Nanomater. Interfaces 118 (2014) 22754–22759.
[47] M.S.A. Khan, I. Ahmad, In vitro antifungal anti-elastase and anti-keratinase activity of essential oils of cinnamomum-, syzygium-and cymbopogon-species against *Aspergillus fumigatus* and *Trichophyton rubrum*, Phytomedicine 19 (2011) 48–55.
[48] K.R. Zodrow, J.D. Schiffman, M. Elimelech, Biodegradable polymer (PLGA) coatings featuring cinnamaldehyde and carvacrol mitigate biofilm formation, Langmuir 28 (2012) 13993–13999.
[49] Y.-S. Chen, Y.-C. Hung, I. Liau, G.S. Huang, Assessment of the in vivo toxicity of gold nanoparticles, Nanoscale Res. Lett. 4 (2009) 858.
[50] I. Fratoddi, I. Venditti, C. Cametti, M.V. Russo, How toxic are gold nanoparticles? The state-of-the-art, Nano Res. 8 (2015) 1771–1799.
[51] D.N. Williams, S.H. Ehrman, T.R.P. Holoman, Evaluation of the microbial growth response to inorganic nanoparticles, J. Nanobiotechnol. 4 (2006) 3.
[52] H.K. Daima, P. Selvakannan, R. Shukla, S.K. Bhargava, V. Bansal, Fine-tuning the antimicrobial profile of biocompatible gold nanoparticles by sequential surface functionalization using polyoxometalates and lysine, PLoS One 8 (2013) e79676.
[53] I.N. Ghosh, S.D. Patil, T.K. Sharma, S.K. Srivastava, R. Pathania, N.K. Navani, Synergistic action of cinnamaldehyde with silver nanoparticles against spore-forming bacteria: a case for judicious use of silver nanoparticles for antibacterial applications, Int. J. Nanomed. 8 (2013) 4721.
[54] J.H. Sung, J.H. Ji, J.D. Park, J.U. Yoon, D.S. Kim, K.S. Jeon, M.Y. Song, J. Jeong, B.S. Han, J.H. Han, Subchronic inhalation toxicity of silver nanoparticles, Toxicol. Sci. 108 (2008) 452–461.
[55] K. Bilberg, M.B. Hovgaard, F. Besenbacher, E. Baatrup, In vivo toxicity of silver nanoparticles and silver ions in zebrafish (*Danio rerio*), J. Toxicol. 2012 (2011).
[56] S. Marin, G. Mihail Vlasceanu, R. Elena Tiplea, I. Raluca Bucur, M. Lemnaru, M. Minodora Marin, A. Mihai Grumezescu, Applications and toxicity of silver nanoparticles: a recent review, Curr. Top. Med. Chem. 15 (2015) 1596–1604.
[57] N.A. Gow, A.J. Brown, F.C. Odds, Fungal morphogenesis and host invasion, Curr. Opin. Microbiol. 5 (2002) 366–371.
[58] Q. Yu, J. Li, Y. Zhang, Y. Wang, L. Liu, M. Li, Inhibition of gold nanoparticles (AuNPs) on pathogenic biofilm formation and invasion to host cells, Sci. Rep. 6 (2016).
[59] W.-R. Li, Q.-S. Shi, H.-Q. Dai, Q. Liang, X.-B. Xie, X.-M. Huang, G.-Z. Zhao, L.-X. Zhang, Antifungal activity, kinetics and molecular mechanism of action of garlic oil against *Candida albicans*, Sci. Rep. 6 (2016) 22805.
[60] K. Hultenby, E. Chryssanthou, L. Klingspor, K. Rensfeldt, L. Strömbeck, J. Faergemann, The effect of K101 Nail Solution on *Trichophyton rubrum* and *Candida albicans* growth and ultrastructure, Mycoses 57 (2014) 630–638.
[61] K. Ikuma, A.W. Decho, B.L. Lau, When nanoparticles meet biofilms—interactions guiding the environmental fate and accumulation of nanoparticles, Front. Microbiol. 6 (2015).
[62] S. Gaidhani, R. Singh, D. Singh, U. Patel, K. Shevade, R. Yeshvekar, B.A. Chopade, Biofilm disruption activity of silver nanoparticles synthesized by *Acinetobacter calcoaceticus* PUCM 1005, Mater. Lett. 108 (2013) 324–327.
[63] X. Li, Y.-C. Yeh, K. Giri, R. Mout, R.F. Landis, Y. Prakash, V.M. Rotello, Control of nanoparticle penetration into biofilms through surface design, Chem. Commun. 51 (2015) 282–285.
[64] J.J. Harrison, H. Ceri, R.J. Turner, Multimetal resistance and tolerance in microbial biofilms, Nat. Rev. Microbiol. 5 (2007) 928.
[65] I.M. Helander, H.-L. Alakomi, K. Latva-Kala, T. Mattila-Sandholm, I. Pol, E.J. Smid, L.G. Gorris, A. von Wright, Characterization of the action of selected essential oil components on Gram-negative bacteria, J. Agric. Food Chem. 46 (1998) 3590–3595.
[66] B. Shafreen, R. Mohmed, C. Selvaraj, S.K. Singh, S. Karutha Pandian, *In silico* and *in vitro* studies of cinnamaldehyde and their derivatives against LuxS in *Streptococcus pyogenes*: effects on biofilm and virulence genes, J. Mol. Recognit. 27 (2014) 106–116.
[67] A.L. Goldberg, Protein degradation and protection against misfolded or damaged proteins, Nature 426 (2003) 895–899.